LEGIBILITY NOTICE

A major purpose of the Technical Information Center is to provide the broadest dissemination possible of information contained in DOE's Research and Development Reports to business, industry, the academic community, and federal, state and local governments.

Although a small portion of this report is not reproducible, it is being made available to expedite the availability of information on the research discussed herein.

LA-UR-

Los Alamos National Laboratory is operated by the University of California for the United States Department of Energy under contract W-7405-ENG-36

TITLE SYNTHESIS OF MATERIALS WITH INFRARED AND ULTRAVIOLET LASERS

LA-UR--88-2740

DE88 016234

AUTHOR(S) J. L. Lyman, CLS-4

SUBMITTED TO Trends in Quantum Electronics, Bucharest, Romania
Aug. 29 - Sept. 3, 1988

DISCLAIMER

Los Alamos National Laboratory
Los Alamos, New Mexico 87545

Synthesis of materials with infrared and ultraviolet lasers

John L. Lyman

Chemical and Laser Sciences Division
Los Alamos National Laboratory
Los Alamos, NM 87545

ABSTRACT

This paper discusses three divergent examples of synthesis of materials with lasers. The three techniques are: (1) Infrared (CO_2) laser synthesis of silane (SiH_4) from disilane (Si_2H_6); (2) Excimer (ArF) laser production of fine silicon powders from methyl- and chloro-substituted silanes; and, (3) Excimer (KrF) laser production of fine metallic powders by laser ablation. The mechanism for each process is discussed along with some conclusions about the features of the laser radiation that enable each application.

1. INTRODUCTION

Synthesis of chemicals and other materials is not yet a common application of lasers, but the potential is high because of some of the unique properties of laser radiation. Some of these properties are not entirely obvious as aids to synthetic procedures. This paper discusses three divergent examples of laser synthesis along with some conclusions about the properties of the laser radiation that enable this application. These properties include wavelength, pulse length, pulse energy, as well as the properties of the laser-heated absorbing material.

Through the late 1970's the major research interest relating to the preparation of materials with lasers was laser isotope separation[1]. Several techniques have been developed, and some are still in a research phase. However, the scope of ideas for applications of lasers has broadened considerably.

The three synthesis techniques discussed in the paper are: (1) Infrared (CO_2) laser synthesis of silane (SiH_4) from disilane (Si_2H_6); (2) Excimer (ArF) laser production of fine silicon powders from silicon chlorides; and, (3) Excimer (KrF) laser production of fine metallic powders by laser ablation.

2. INFRARED LASER SYNTHESIS OF DISILANE FROM MONOSILANE

A research group at the AMOCO Technology Company has demonstrated[1-3] conversion of SiH_4 to Si_2H_6 with high yield and high purity. More conventional methods of synthesis[1], such as reduction of hexachlorodisilane with lithium aluminumhydride, electrical discharge in silane, or hydrolysis of magnesium silicides, all produce low yields of the desired disilane and a considerable quantity of both volatile and nonvolatile silicon compounds.

A major reason for wishing to convert silane to disilane is for its use in chemical vapor deposition (CVD). With disilane as the silicon source, thermal CVD is possible at temperatures more than 100 K lower than with silane as the source[4]. The resulting silicon has better adherence and electronic properties.

2.1. Experimental procedure and results

The synthetic process involves the irradiation of high pressure silane gas with a pulsed carbon dioxide laser. For optimum conditions the disilane product yield is high, the selectivity is high, and the energy efficiency is high. Disilane is virtually the only volatile, silicon-containing product. (Hydrogen is the other volatile product.)

A previously published study by Longeway and Lampe[5] showed that when silane is irradiated by a carbon dioxide laser pulse at low pressure (less that 20 torr) only a small amount of disilane is produced and that the disilane is only a small part of the volatile, silicon-containing products. Higher pressures significantly change the product distribution.

The experiments were performed with absorption cells of different lengths. Each was of aluminum construction with sodium chloride windows. All laser irradiations were with TEA CO_2 laser operating at the 10P20 line (944.19 cm^{-1}) at up to 1.2 J/pulse. Most experiments were performed by irradiating the samples of gaseous silane for many pulses followed by a product analysis by gas chromatography. Analysis of the irradiated samples gave the disilane yield, the silane consumed, the reaction selectivity (disilane produced / silane consumed), and the energy efficiency (disilane yield x energy required for silane dissociation / energy absorbed).

Successive irradiation of a silane sample generates the product disilane (fig. 1). Eventually, as the disilane accumulates the disilane consumption rate equals the production rate, and the product ceases to increase. The lower thermal stability of the disilane is one of its

advantages as a CVD reagent. However, this means that it must be removed from the reaction zone as it accumulates.

The experiments for fig. 1 were at 100 torr. The decomposition of disilane becomes less critical at higher pressures. Figure 2 show the pressure dependence for disilane synthesis for two different laser energies. Note that the large volume of this cell allows the disilane to diffuse out of the irradiation region between the pulses. The fraction of the cell irradiated decreases with increasing pressure because of the reduction of the absorption pathlength. This partially accounts for the increase of yield with pressure. The higher energy laser pulses give a stronger dependence of the product yield on pressure. The high energy absorbed per molecule and the lower collisional stabilization rate at low pressure contribute to this stronger dependence.

The selectivity for production of disilane was high for the experiments of fig. 2. The selectivities fell in the range of 0.25 to 0.40 (0.50 is perfect selectivity) for the entire range of experiments. The energy efficiency, on the other hand, increased monotonically from about 0.006 at low pressure to 0.13 at 1000 torr. These results suggest that at low pressure considerable decomposition of the reaction products occurs back to the initial silane reagent.

In a series of experiments with a smaller cell and many more laser pulses the dependence of the reaction yield on pressure was similar to fig. 2. The selectivity, however, depended linearly on pressure (fig. 3). For these experiments the number of laser pulses was well beyond that necessary to bring the reaction mixture to a steady state condition (fig. 1). The low selectivity at low pressure indicates that not only do the products revert back to silane, but the reaction tends to continue to higher silanes and eventually to solid products.

2.2. Reaction mechanism

The chemical reaction mechanism proposed by Longeway and Lampe[5] successfully accounts for the experiments discussed here. Figure 4 summarizes the essential features of the reaction mechanism. The first step is the laser excitation of silane. Collisions play an important role in the absorption processes[6]. At low pressures absorption is limited by the rate of rotational energy transfer into absorbing states and out of vibrationally excited states. Collisional broadening also contributes to the increase of of absorption cross section (fig. 5) up to about 200 torr and the decrease above that pressure. Collisionally induced vibrational energy transfer also contributes to the absorption process in a minor way.

The vibrationally-excited silane produced by laser absorption or by collisional redistribution of internal energy may either dissociate or become collisionally stabilized. The SiH_2 reaction product inserts rapidly into chemical bonds. When SiH_4 is the major species, the bond-insertion reaction produces a highly vibrationally-excited disilane molecule. Three reactions are available to this excited molecule. The first is the elimination of the SiH_2 radical. This is the reverse of the formation reaction. This reaction does not influence the selectivity, but its occurrence does reduce the energy efficiency. It is probably a major contributor to the low energy efficiency at low pressure. The second possible reaction is H_2 elimination. This reaction leads to higher silanes and solid products. The resulting radical, SiH_3SiH, may also insert into chemical bonds. The competition between this reaction and the third possibility, collisional stabilization, determines the reaction selectivity.

Collisional stabilization is the desired reaction for efficient synthesis. The fact that the rate of this reaction increases with pressure is the major reason that high pressures favor the synthesis. In many laser applications, such as laser isotope separation, collisional processes are detrimental. This is not the case for disilane synthesis. High yields result only if the pressure of silane is greater than 75 torr, and high purity synthesis is possible at pressures as high as 1500 torr.

2.3. Cooling of the reacting gas

In the absence of some process that can cool the reacting gas, the less stable disilane product would continue to decompose. Fortunately, the near adiabatic expansion of the hot gas cools the reacting mixture on the desired time scale. Conduction cooling to the cell window may also occur. However, this process is too slow for all pressures. The closer proximity of the window at high pressures is offset by the lower conduction rate. The expansion cooling occurs on the time scale of the acoustical transit time in the hot gas. Figure 6 shows a calculation of this type of expansion. The vertical axis is the peak temperature anywhere in the irradiated region. The calculation also includes conduction cooling, but it is significant only very near the window. Here again the smaller reaction volume and faster cooling time at high pressure partially offsets the faster reaction at high pressure.

2.4. Summary of critical processes in disilane synthesis

The time required for heating, reaction, and cooling of the sample is critical in the laser synthesis of disilane. Rapid (laser) heating, rapid (but not complete) reaction, and rapid cooling all contribute to the high yields.

To summarize, the proposed mechanism of the photochemical reaction includes: (1) Collisionally-enhanced absorption of the laser radiation by silane; (2) Collisional de-excitation of the vibrationally excited silane; (3) Concurrent decomposition to SiH_2 and H_2; (4) Production of vibrationally excited disilane by SiH_2 insertion into a silane Si-H bond; (5) Collisional quenching of the excited disilane; and (6) Rapid cooling of the irradiated gas by thermal expansion. Collisions contribute to the synthesis by enhancing absorption, by stabilizing the excited disilane, and by vibrational-to-translational energy transfer, which terminates the reaction by removing energy from the vibrational degrees of freedom and by cooling the gas by adiabatic expansion.

3. LASER PRODUCTION OF FINE SILICON POWDERS

Silicon powder is a useful material for sintering into monolithic components. The material that is used most often for a feedstock for production of silicon powder is silane. It has the advantages of being a gas at room temperature and being thermally less stable than the products silicon and hydrogen. However, it is considerably more expensive than several methyl- and chloro-substituted silanes. The group at the Centre for Industrial Laser Applications (CILA), University of New South Wales, has demonstrated that excimer laser (ArF, 193 nm) irradiation of gaseous species of this general type ($SiH_k(CH_3)_m Cl_n$, n>0), produces fine silicon powders. This process could have significant economic advantage over similar processes with silane.

3.1. Experimental procedure and results

The powder was produced by irradiating a stream of one of the compounds with an ArF excimer laser. The ArF laser had a pulse length of approximately 20 ns with pulse energy near 35 mj and a repetition rate of 100 Hz. The gas stream was created by heating a flask of the liquid and passing the vapor through a rectangular nozzle 1 cm by 1 mm. The irradiation was along the long dimension just as the stream exited the nozzle. The laser beam size at the nozzle was 1 mm by 4 mm. The transverse flow of the irradiated gas was such that each pulse irradiated new gas. All of the silicon compounds used absorbed the 193 nm laser radiation.

The laser irradiation produces fine silicon powders (20-40 nm dia. with some larger agglomerates in the 200-300 nm range). Experiments with eight different species gave quantum yields (silicon atoms in the powder per photon absorbed) in the range of 0.2 to 0.9. Table 1 shows the compounds used and the measured quantum yield for powder production. Species without methyl groups ($SiCl_4$ and $SiCl_3H$) required addition of hydrogen for powder production.

3.3. Model development for experimental analysis

For simplicity $SiCl_4$ with H_2 was selected for the initial modeling effort. Most experiments were at 100 torr mixtures with $[H_2]/[SiCl_4]=2$. The measured energy absorbed exceeded that calculated from the small signal absorption cross section (4.8×10^{-20} cm^2) by about 20%. Experiments with $SiCl_4$ required hydrogen for powder production.

The model contains laser absorption processes. literature values[8-10] of some thermodynamic and physical properties, proposed chemical reactions, and both measured and estimated rate constants. Some rate constants were available in the literature[9,10] (Cl/H system). Others were estimated by consideration of similar reactions, unimolecular reaction rate theory, and thermodynamic constraints. Sufficient thermodynamic data[8] is available for the model to have correct equilibrium constants. The model accounts for the available experimental data. It is certainly not a unique explanation of the experimental results, but it does lead to some tentative conclusions and suggestions for further study.

The conclusions fall into two categories. The first is a list of observations and conclusions supported by experimental evidence. The second is a list of model features that is consistent with experimental data and other constraints, but that requires additional experimental verification.

3.3.1. Observations and conclusions supported by experimental evidence

1. The average number of photons absorbed per molecule is about 0.04.

2. Laser-induced breakdown does not occur.

3. Absorption by photofragments ($SiCl_3$, $SiCl_2$, $SiCl$) or multiphoton processes may occur, but these do not dominant the absorption mechanism.

4. Absorption of the laser radiation leads to one of two dissociations reactions,

$$SiCl_4 \text{ ----> } SiCl_3 + Cl$$

or

$$SiCl_4 \text{ ----> } SiCl_2 + Cl_2 \ .$$

5. Recombination reactions like

$$SiCl_3 + Cl \text{ ----> } SiCl_4$$

are more rapid than the successive reactions that lead to silicon powder.

3.3.2. Model features requiring additional experimental verification:

1. Exchange reactions like

$$SiCl_3 + SiCl \text{ ----> } SiCl_4 + Si$$

occur.

2. Initial Si/Cl clusters form and continue to grow by radical recombination, and bond insertion reactions,

$$Si_jCl_j + Si_nCl_m \text{ ----> } Si_{j+n}Cl_{j+m} \quad .$$

3. Clusters reduce Cl/Si ratio by $SiCl_4$ elimination,

$$Si_nCl_m \text{ ----> } Si_{n-1}Cl_{m-4} + SiCl_4 \quad ,$$

and by chlorine abstraction reactions,

$$Si_nCl_m + SiCl_3 \text{ ----> } Si_nCl_{m-1} + SiCl_4 \quad .$$

4. Hydrogen reduces recombination by scavenging atomic chlorine,

$$Cl + H_2 \text{ ----> } HCl + H$$

5. Atomic hydrogen forms new reactive silicon species,

$$SiCl_4 + H \text{ ----> } SiCl_3 + HCl \quad ,$$

and reduces chlorine content of clusters,

$$Si_nCl_m + H \text{ ----> } Si_nCl_{m-1} + HCl \quad .$$

6. Agglomeration of larger clusters,

$$Si_jCl_k + Si_nCl_m \text{ ----> } Si_{j+n}Cl_{k+m} \quad ,$$

requires both low chlorine content and high internal energy.

7. The maximum translational temperature is below 600 K.

3.3.3 Additional work necessary to clarify the reactions mechanism

Confirmation of the mechanism of cluster formation would require considerably more experimental work, such as: measurement of the rate of cluster growth by Mie scattering

or some other technique; determination of the chlorine content of the clusters, particularly in the early stages of formation; a careful measurement of the intensity distribution (spatial) in the irradiated region; independent measurement of the rate constants for almost any of the reactions mentioned above; and, measurement of the electron density and temperature.

4. FINE POWDER PRODUCTION BY LASER ABLATION OF METALS

Fine metallic powders have a number of commercial applications, such as catalysts for chemical processes. The CILA[11-13] group has generated powders of nickel, platinum, tantalum, and copper by laser ablation of the solid metal. They have also measured the catalytic activity of the nickel powders. A one-dimensional model of ablation process gives some insight into the process of the laser interaction with the metal surface.

4.1. Experimental approach and results

The experimental program[12,13] involves irradiation of a rotating metal target with focused excimer laser pulses (KrF, 248 nm). In these experiments the laser pulse energy was 180 mJ, the pulse length 20 ns, and the repetition rate 100 Hz. The yield of the ablated powder was determined by either measuring the mass or the collected powder or by measuring the mass loss of the solid target.

The yield and conformation of the ablated material depend strongly on the pressure of the argon gas over the metal surface. At low pressures (below 1 torr) the ablated metal forms a mirror on the walls of the collecting cylinder. For higher pressures powders form with most particle diameters between 2 and 10 nm and a few in the 100 nm range.

The powder yield[13] decreases with increasing pressure. Figure 7 shows the variation of yield with pressure of argon above the metal surface for platinum, copper, and nickel. (The yields for tantalum are between those for platinum and copper.) Note that all of these metals show similar trends with the pressure of the argon above the metal surface. Above about 10 torr the powder yield tends to fall off with pressure.

Smaller spot sizes[12] also increase the powder yield. The optimum appears to be about 0.33 mm^2. This was the beam area for most of the experiments.

The catalytic activity of the metallic powders is excellent. Several tests[13] were made to compare the catalytic activity of the laser-produced nickel powder with a commercial nickel catalyst. The commercial catalyst was Raney nickel catalyst powder, an alloy of 50% nickel and 50%

aluminum. The test reaction was hydrogenation of propene to propane. The laser-produced nickel had five times the catalytic activity of the the Raney nickel.

4.2. Modeling the nickel ablation processes

Nickel was selected for computer simulation of the ablation process because of the availability of physical constants and experimental data.

The computer simulation of the experiments is a one-spatial-dimension numerical solution of conservation equations for energy, momentum, nickel density, and argon density. The single spatial dimension is perpendicular to the metal surface. The computation algorithm is an adaptation of the SOLA-ICE method[14]. Table 2 gives the physical constants and thermodynamic data used by the model. Both the specific heat and the solid thermal conductivity are fits to the published data. Based on comparisons with copper and aluminum, the thermal conductivity for liquid nickel was assumed to be 40% of the solid value. Both the gas-phase thermal conductivity and the diffusion coefficient were calculated from hard-sphere kinetic-theory expressions. The vapor pressure, assumed to have Arrhenius form, was obtained from the heat of vaporization and the boiling point.

The computer solution accounts for absorption of the laser radiation and gives the temperature, nickel density, argon density, pressure, and vapor velocity as functions of time and position. In the vapor phase expansion, contraction, diffusion, and gas movement may occur. Changes in the condensed phases include thermal conduction and phase changes (the magnetic transformation at the Curie point, melting, and freezing). Evaporation and condensation occur only at the solid vapor interface. The evaporization (or condensation) rate was assumed to be fast enough to maintain the nickel partial pressure at the vapor pressure for the local temperature.

The experimental laser pulse length was 20 ns. The model pulse shape was a half Gaussian (beginning at the peak) with a width (1/e) of 20 ns. The published values[15,16] for surface reflectance and light penetration into the condensed material give the rate and spatial distribution absorption of the laser radiation. For most calculations absorption of the laser energy occurs only in the condensed phases (solid/liquid) near the surface. This is somewhat unrealistic, however, because as the metal evaporates rapidly, it remains at a very high density. This high density vapor will certainly absorb some of the laser energy. Furthermore, a plasma may form in the hot vapor, which will strongly absorb the laser radiation. To partially account for these absorption processes, one set of

calculations was performed with the absorption coefficient of the nickel vapor decreasing from its solid-phase value with the square root of the density.

Figures 8-11 show the results of calculations where absorption is entirely by the condensed phases. The calculations are at two times, 5 ns and 100 ns. The first time is early in the laser pulse and the latter is well after the end of the pulse. The spatial range in the graphs is over the entire range for temperature (Figs. 8 and 10) and only in the vapor range for the other quantities.

Figure 12 shows how the nickel vapor density develops when absorption occurs in the vapor phase as well as in the condensed phases. In all computations the strong shocks that develop as the vapor expands from the surface tend to generate numerical instabilities. This is a major contributor to some of the rough curves between the surface and the shock front.

As the temperature of metal surface increases, the material begins to evaporate. The vapor pressure, temperature, and vapor density control the rate of evaporation. In the current version of the model an ideal gas equation of state was assumed for the nickel vapor. One suggestion for improvement of the model is to replace this assumption with a more realistic equation of state.

At 5 ns (Figs. 8,9) some of the nickel near the surface has exceeded the Curie point, the melting point, and the boiling point and has begun to evaporate from the surface. The absorption of the laser energy is accompanied by a very rapid rise in temperature and pressure. This results in the formation of a strong shock wave that moves out from the surface. The shock formation is more apparent at the longer times (100 ns, Figs. 10,11). At 5 ns the shock velocity is 2×10^5 cm/s, or Mach 6, by 100 ns the velocity at the shock front has dropped to about Mach 3. Evaporation is still occurring at 100 ns. (The velocity at the surface is still positive, but it is reduced considerably from the high value during the laser pulse. The slower evaporation rate results in a high-density slug of nickel vapor near the shock front. The ambient argon gas gets pushed to high density in front of the much-higher-density nickel vapor. The experimental decrease of yield with increasing pressure is most likely due to the argon gas holding the evaporating material near the surface. This slows the expanding nickel vapor, retards evaporation at the surface, and allows some of the material to recondense as the surface cools by conduction and radiation.

The metal vapor that escapes from the surface will continue to cool and expand. At some point the cooling plume will begin to form atomic clusters. (This process is

not yet a part of the model.) If the argon confinement is sufficient, the nucleation process results in the fine powders. At low argon pressures the confinement and heat transfer is insufficient to form the clusters and a mirror plating on the vessel surface results.

If we assume that all of the evaporated material eventually forms powder, then the model overestimates the yield by about a factor of 20. The main contributions to the differences between the experiments and model calculations are the use of the ideal-gas equation of state for the nickel, the lack of a good model for absorption in the vapor phase, the difficulty of measuring the laser spot size, and the absence of a nucleation model for cluster formation.

Laser ablation produces very small particles. Some of this is due to the competitive dynamics of expansion and nucleation. However, Robers[19] has suggested that cluster ionization and the resulting repulsive forces will tend to keep the clusters small. The ionization occurs by both thermal ionization processes and photoelectron effects.

Two suggestions mentioned above for improving the model were a more realistic treatment of the equation of state and a better model for absorption by evaporated nickel. Other suggestions include: a treatment of plasma formation, inclusion of laser absorption by the plasma, addition of particle growth from the atomic vapor, inclusion of measured reflectance at high intensities, and consideration of secondary radiative-transport processes.

5. CONCLUSIONS

The three laser synthetic processes considered in this paper require different properties of the lasers involved and the materials being processed. For the disilane synthesis with infrared laser pulses the collisional processes were probably the most important. The molecular collisions both enabled the absorption of laser radiation and stabilized the reaction product by vibrational energy transfer and expansion cooling.

The silicon powder production from silicon-containing gases required a laser (ArF) with a wavelength that was strongly absorbed by the gases. The complex chemical reactions that occurred after the laser pulse were also important.

The powder production by metal ablation with an excimer (KrF) laser required a short, energetic laser pulse. The wavelength was almost irrelevant. However, the high heating

rates and the resulting high pressures were necessary to evaporate the metal and expel it from the surface.

All three of these processes have technological potential. Their utilization will depend on the demand for the respective products.

6. ACKNOWLEDGMENTS

The author wishes to thank J. A. O'Neill, M. Horsburgh, J. Tann, W. Sinclair, G. Paul, G. Keen, C. J. Russell, and J. Zavelovich for prepublication access to their work and the US Department of Energy, Los Alamos National Laboratory, Amoco Technology Company, and The University of New South Wales Centre for Industrial Laser Applications for their support of this work.

7. REFERENCE

1. J. L. Lyman, "Laser-induced molecular dissociation. Application to isotope separation and related processes," in Applications of Lasers and Spectroscopy, I. J. Radziemski, R. W. Solarz, and J. A. Paisner, eds., Marcel Dekker, Inc., 417-505 (1987).

2. J. Zavelovich and D. S. Hacker, "Photochemical process for preparation of disilane," U. S. Patent, No. 4,604,274, Aug. 5, 1986.

3. J. Zavelovich and J. L. Lyman, "Photochemical Synthesis of Disilane from Silane with Infrared Laser Radiation," J. Phys. Chem. (submitted for publication).

4. S. S. Hegedus, R. E. Rocheleau, W. Buchanan, and B. N. Baron, "Performance and analysis of amorphous silicon p-i-n solar cells made by chemical-vapor deposition from disilane," J. Appl. Phys. 61 (1), 381-389 (1987).

5. P. A. Longeway and F. W. Lampe, "Infrared multiphoton decomposition of monosilane," J. Amer. Chem. Soc, 103 (23), 6813-6818 (1981).

6. J. L. Lyman, J. M. Telle, and R. C. Eckhardt, "The Effect of Collisions of Vibrational Energy Distribution in Polyatomic Molecules," Spectrochim. Acta 43A (2), 141-148 (1987).

7. J. A. O'Neill, M. Horsburgh, J. Tann, and W. Sinclair, "Production of Fine Ceramic Powders from Chloromethyl Silanes Using Pulsed Excimer Radiation," J. Am. Ceram. Soc. (in press).

8. M. W. Chase, Jr, C. A. Davies, J. R. Downey, Jr., D. J. Frurip, R. A. McDonald, and A. N. Syverud, "JANAF thermochemical tables, third edition", J. Phys. Chem. Ref. Data, Suppl. 1, 14, (1985).

9. J. M. White, "Other reactions involving halogen, nitrogen, and sulfur compounds," in Comprehensive Chemical Kinetics, Vol. 6, C. H. Bamford and C. F. H. Tipper, eds., Elsevier Pub. Co., Amsterdam, 201-270 (1972).

10. J. A. Kerr, "Metathetical reactions of atoms and radicals," in Comprehensive Chemical Kinetics, Vol. 18, C. H. Bamford and C. F. H. Tipper, eds., Elsevier Pub. Co., Amsterdam, 39-109 (1976).

11. G. L. Paul, C. J. Russell, G. R. Keen, J. L. Lyman, and J. A. O'Neill, "Ultrafine Powder Production by Excimer Laser Ablation of Metals," (manuscript in preparation).

12. "BHP Progress Report No. 8, January 8, 1987, Laser Manufactured Catalysts," Centre for Industrial Laser Applications, School of Physics, The University of New South Wales, Sydney, Australia.

13. G. Keen, "BHP Progress Report No. 9, November 1987, Laser Manufactured Catalysts," Centre for Industrial Laser Applications, School of Physics, The University of New South Wales, Sydney, Australia.

14. L. D. Cloutman, C. W. Hirt, and N. C. Romero, "SOLA-ICE: A Numerical Solution Algorithm for Transient Compressible Fluid Flows," Los Alamos Scientific Laboratory Report #LA-6236, February 1976.

15. W. Betteridge, Nickel and its Alloys, Halstead Press, New York (1984).

16. Y. S. Touloukian, Thermophysical Properties of Matter, Vol 1, IFI/Plenum, New York (1970).

17. J. O. Hirschfelder, C. F. Curtiss, and R. B. Bird, Molecular Theory of Gases and Liquids, John Wiley & Sons, Inc., New York, 14 (1954).

18. American Institute of Physics Handbook, 3rd ed, McGraw Hill, New York (1982).

19. W. Robers, "Thermische und Elektrische Effekte bei Laserinduzierten Oberflachenreaktionen," Max-Planck-Institut fur Quantenoptik, MPQ 132, Feb. 1988.

TABLE 1

Silicon powder quantum yields from substituted silanes

Feedstock	Quantum Yield	
$Si(CH_3)_4$	0.80	
$Si(CH_3)_3Cl$	0.32	(SiC)
$Si(CH_3)_2Cl_2$	0.59	
$SiCH_3Cl_3$	0.28	
$SiCl_4$	0.00	(0.84 with H_2)
$SiCl_3H$	0.00	(0.22 with H_2)
$Si(CH_3)_2ClH$	0.57	
$SiCH_3Cl_2H$	0.51	

TABLE 2

Physical and thermodynamic data used in the nickel model

Constant	Value	Ref.
Solid Ni Density	8.9 g/cm^3	15
Curie Point	631 K	15
Melting Point	1726 K	15
Boiling Point	3183 K	15
Heat of Magnetic Transformation	0.139 kcal/mol	15
Heat of Fusion	4.10 kcal/mol	15
Heat of Vaporization	89.46 kcal/mol	15
Thermal Conductivity (Solid)	$0.638 \lvert T-631 \rvert^{0.0376}$ W/cm/s	16
Thermal Conductivity (Liquid)	0.250	est.
Thermal Conductivity (vapor)	$3.59 \times 10^{-9} T^{1.5}$	17
Diffusion Coefficient (Ni/Ar)	$0.014 T^{1.5}/p$ cm^2/s	17
Specific Heat	$0.126 T^{0.215}$ cal/K/mol	16
Absorption Coefficient (s/l)	1.17×10^6 cm^{-1}	16,18
Reflectivity (s/l)	0.43	16,18

Figure Captions

1. Concentration of disilane produced versus the number of laser pulses at 0.9 J/pulse and 2 Hz repetition rate for 100 torr initial silane pressure. Experiments were with the long cell, and the analysis was by gas chromatography.

2. Disilane yield versus initial silane pressure for two different values of the pulse energy, 200 pulses at 1 Hz. Experiments were with the long cell.

3. Selectivity of the disilane synthesis versus initial silane pressure for the experiments with 0.56 J/pulse with a smaller volume cell.

5. Silane absorption cross section (points) versus pressure measured with CO_2 in the fluence range 6 to 10 mJ/cm^2, 0.17 cm pathlength. The curve is a calculation based on the absorption model described in the text

6. A hydrodynamic model calculation of the dependence of the peak temperature on time for a 200 torr silane sample irradiated with 0.5 J. cm^2.

7. Metal powder yields versus argon pressure for KrF laser pulse energies near 180 mJ/pulse.

8. Model calculation of temperature versus distance perpendicular to the nickel surface at 5 ns for 55 J/cm^2 and 100 torr argon. Before the laser pulse the solid nickel was $2x10^{-4}$ cm and below, and argon was above $2x10^{-4}$ cm.

9. Nickel density, argon density, and vapor velocity at 5 ns from the calculations of fig. 8.

10. Model calculation of temperature versus distance perpendicular to the nickel surface at 100 ns for 55 J/cm^2 and 100 torr argon. The initial solid/gas boundary was at $2x10^{-3}$ cm.

11. Nickel density, argon density, and vapor velocity at 100 ns from the calculations of fig. 10.

12. Model calculation of nickel density versus distance at several times for conditions similar to figs. 8-11 but with absorption by the nickel vapor.

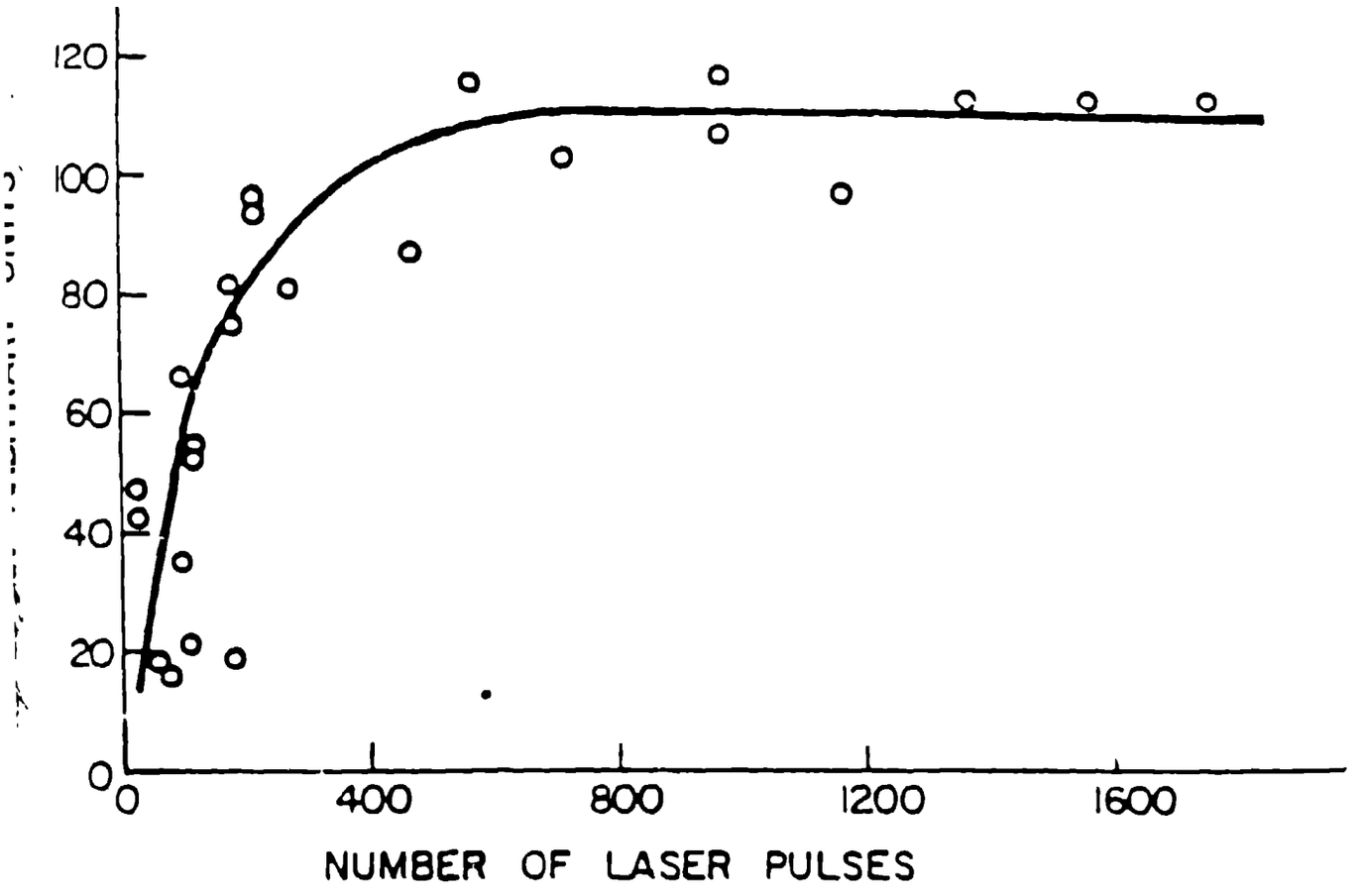

Fig 1

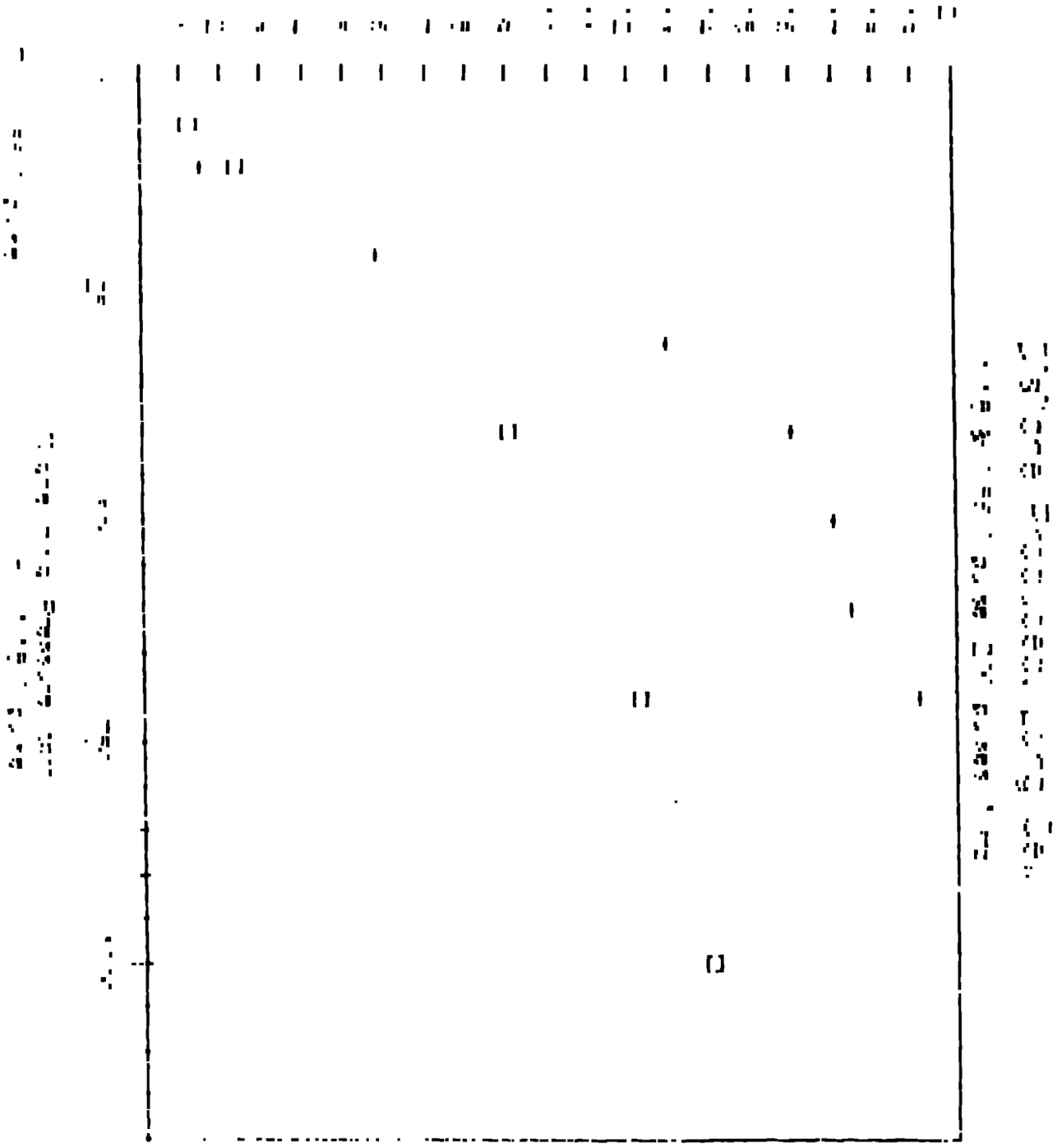

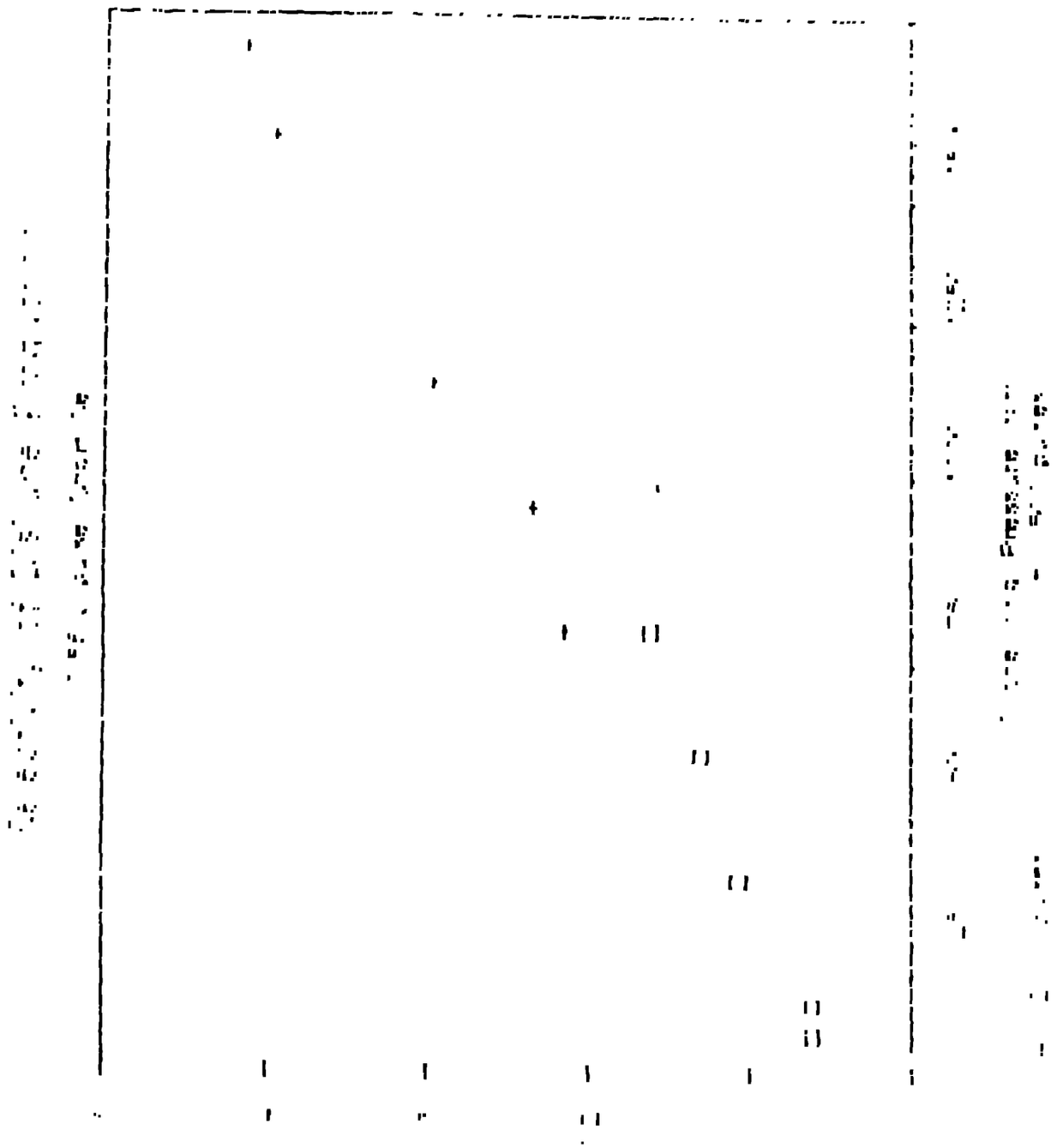

HIGH PRESSURES FAVOR DISILANE PRODUCT IN LASER EXCITATION OF SILANE

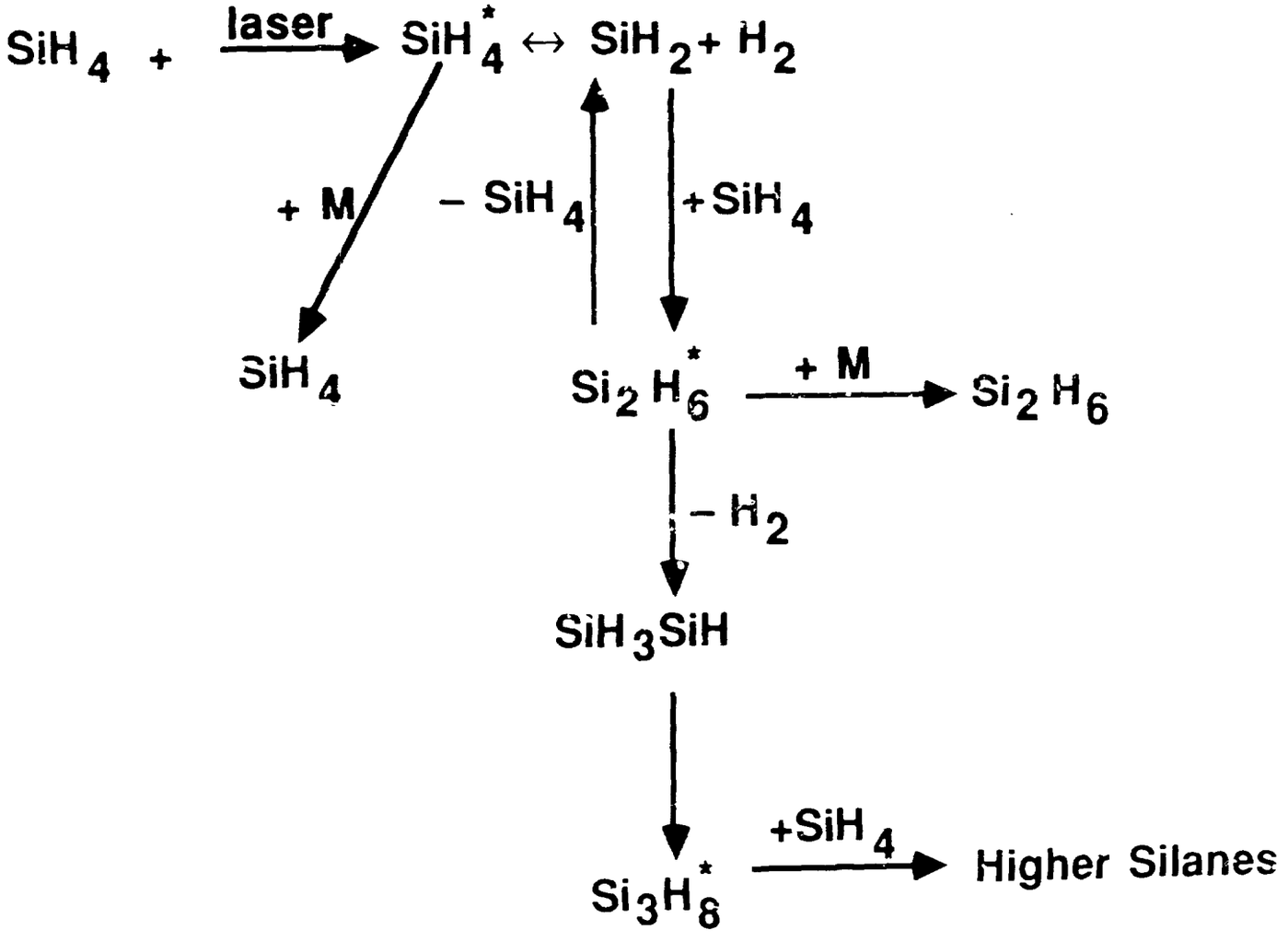

CLS-88-5206

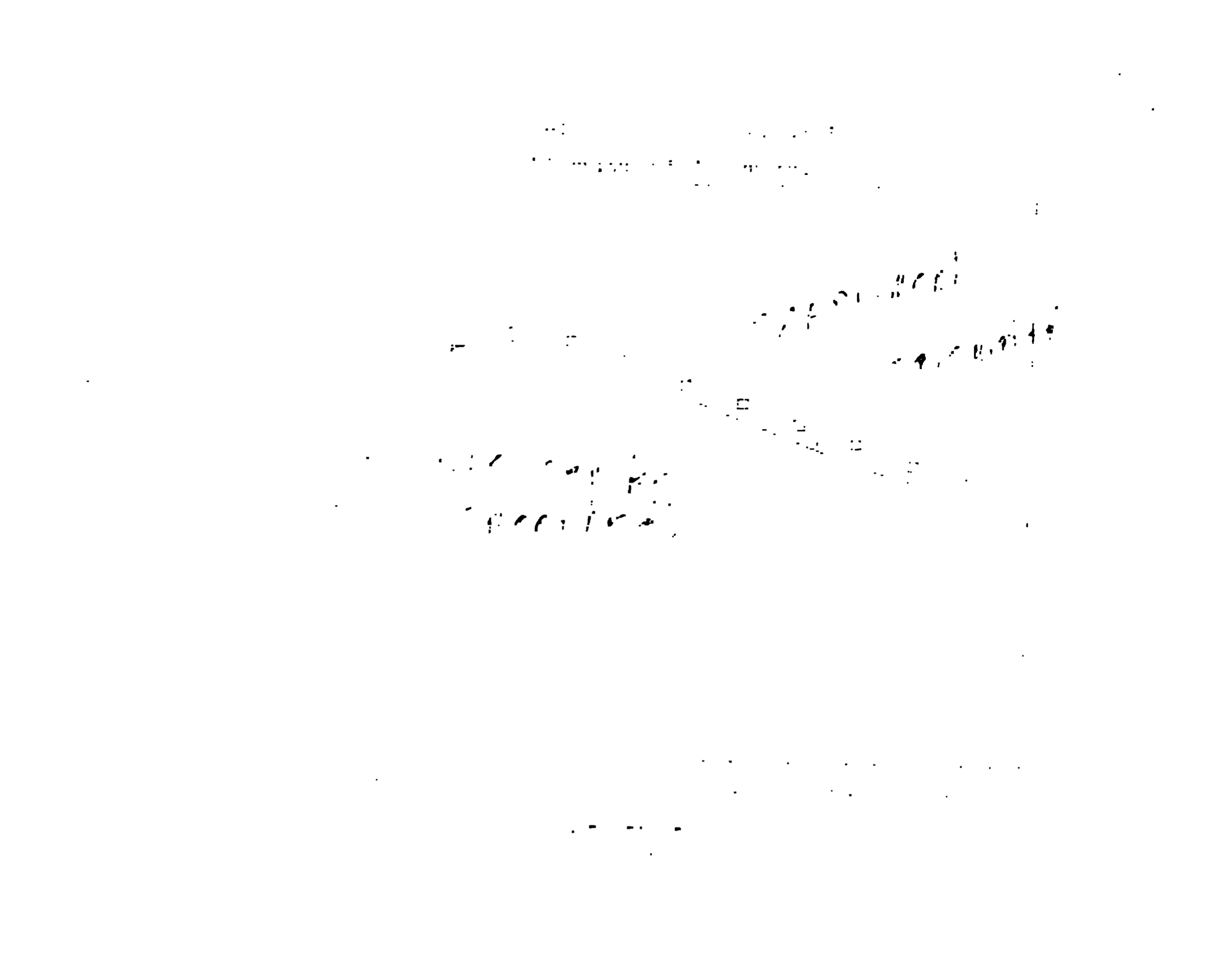

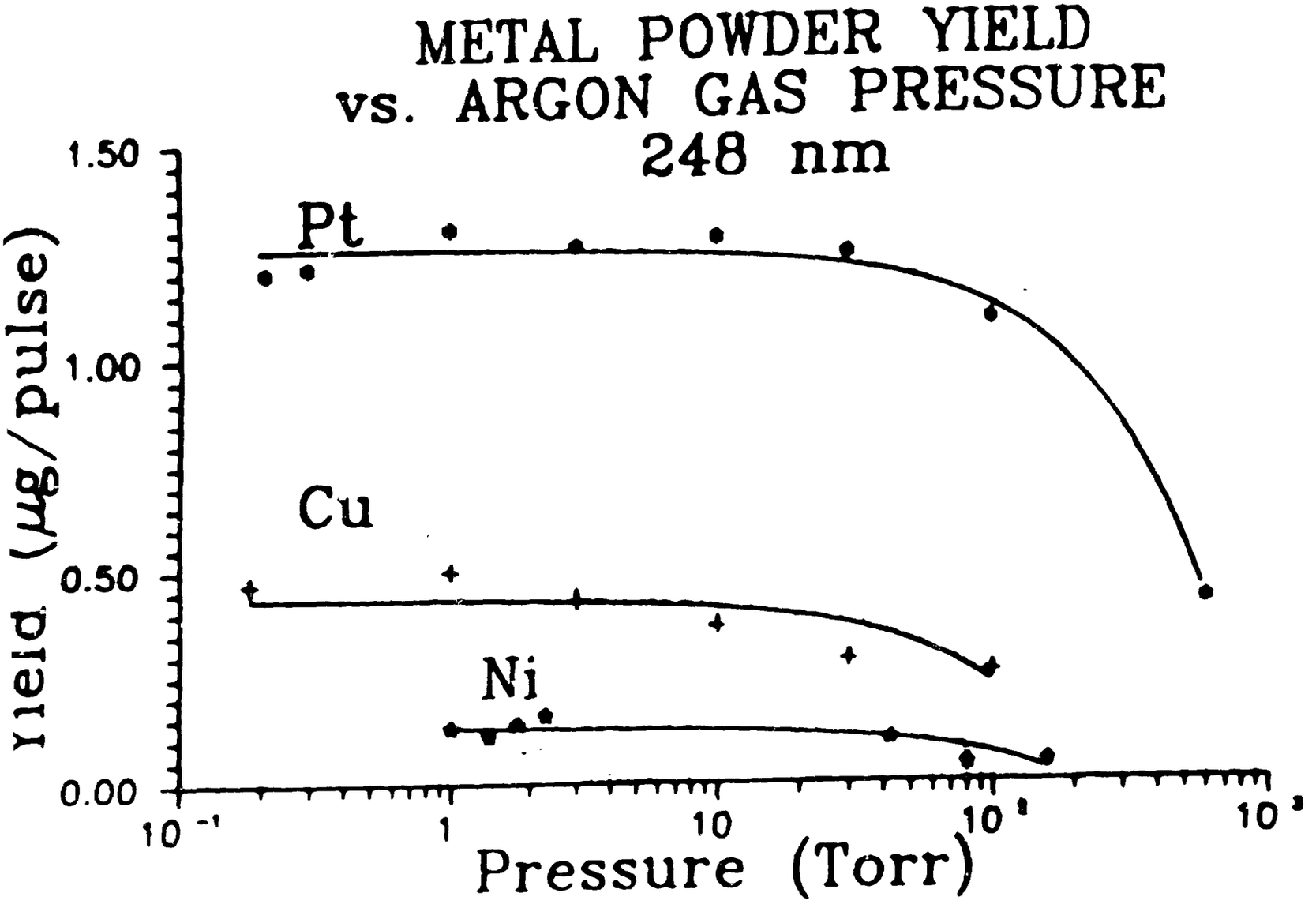
METAL POWDER YIELD
vs. ARGON GAS PRESSURE
248 nm
1.50
1.00
0.50
0.00
Yield (μg/pulse)
Pt
Cu
Ni
10 -1
1
10
10 2
10 3
Pressure (Torr)

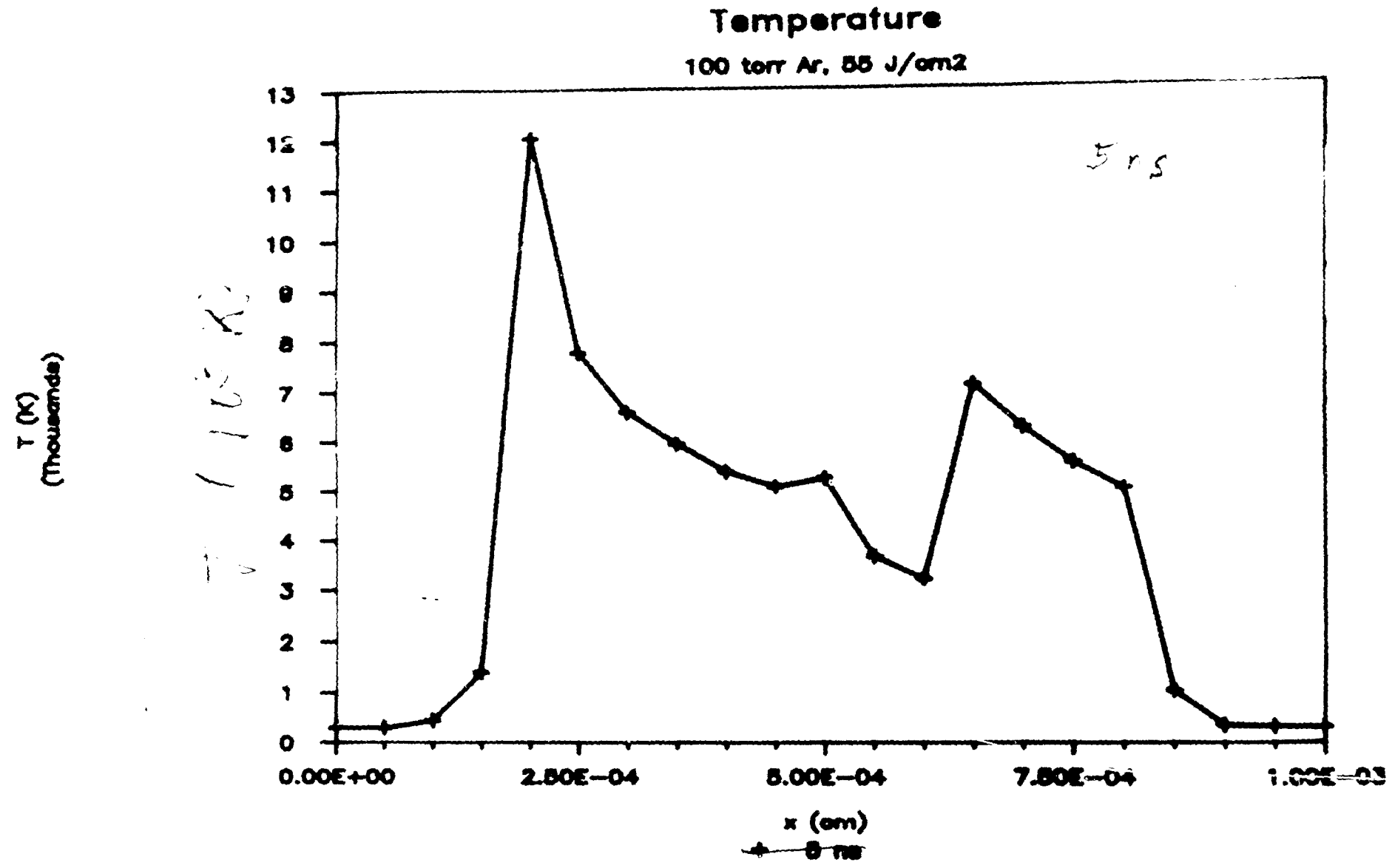
Temperature
100 torr Ar, 55 J/cm2
T (K)
(Thousands)
13
12
11
10
9
8
7
6
5
4
3
2
1
0
0.00E+00
2.50E-04
5.00E-04
7.50E-04
1.00E-03
x (cm)
5 ns
8 ns

5 ns
N (molec/cm3)
(Times 1E21)
Ar (molec/cm3)
(Times 1E18)
v (cm/s)
(Thousands)
x (cm)

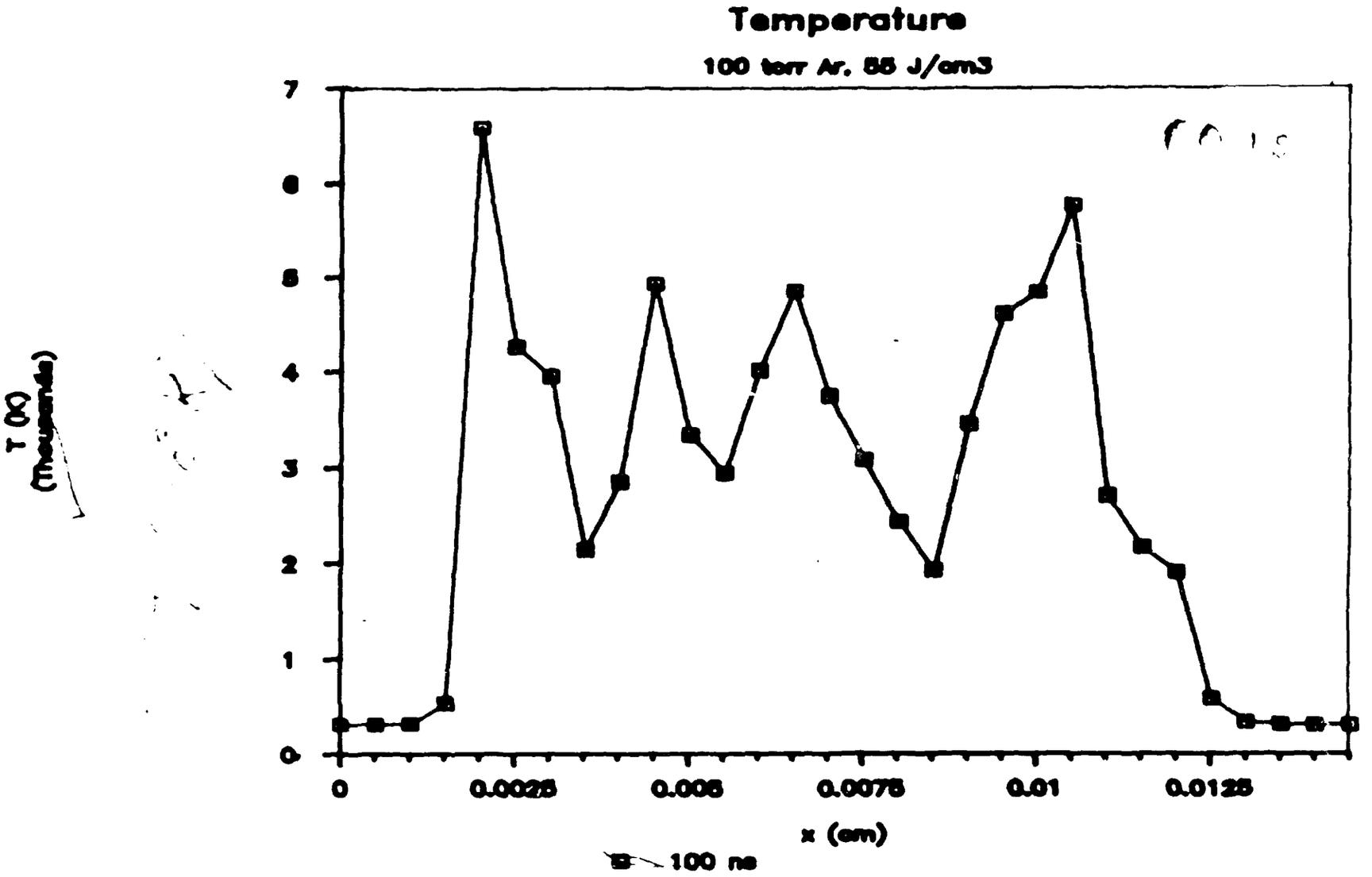
Temperature
100 torr Ar, 55 J/cm3
T (K)
(Thousands)
7
6
5
4
3
2
1
0
0
0.0025
0.005
0.0075
0.01
0.0125
x (cm)
100 ns

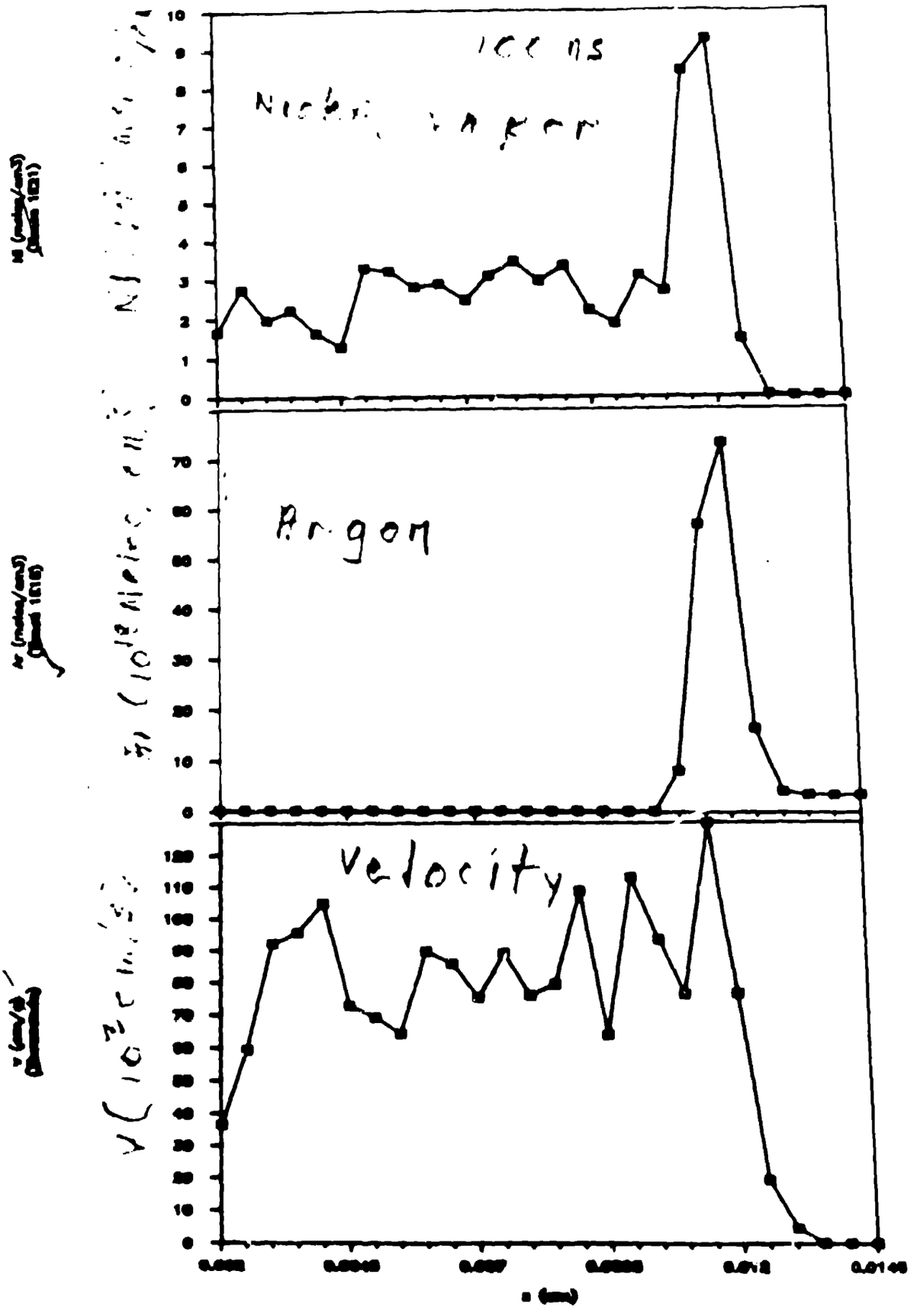
Argon
Velocity

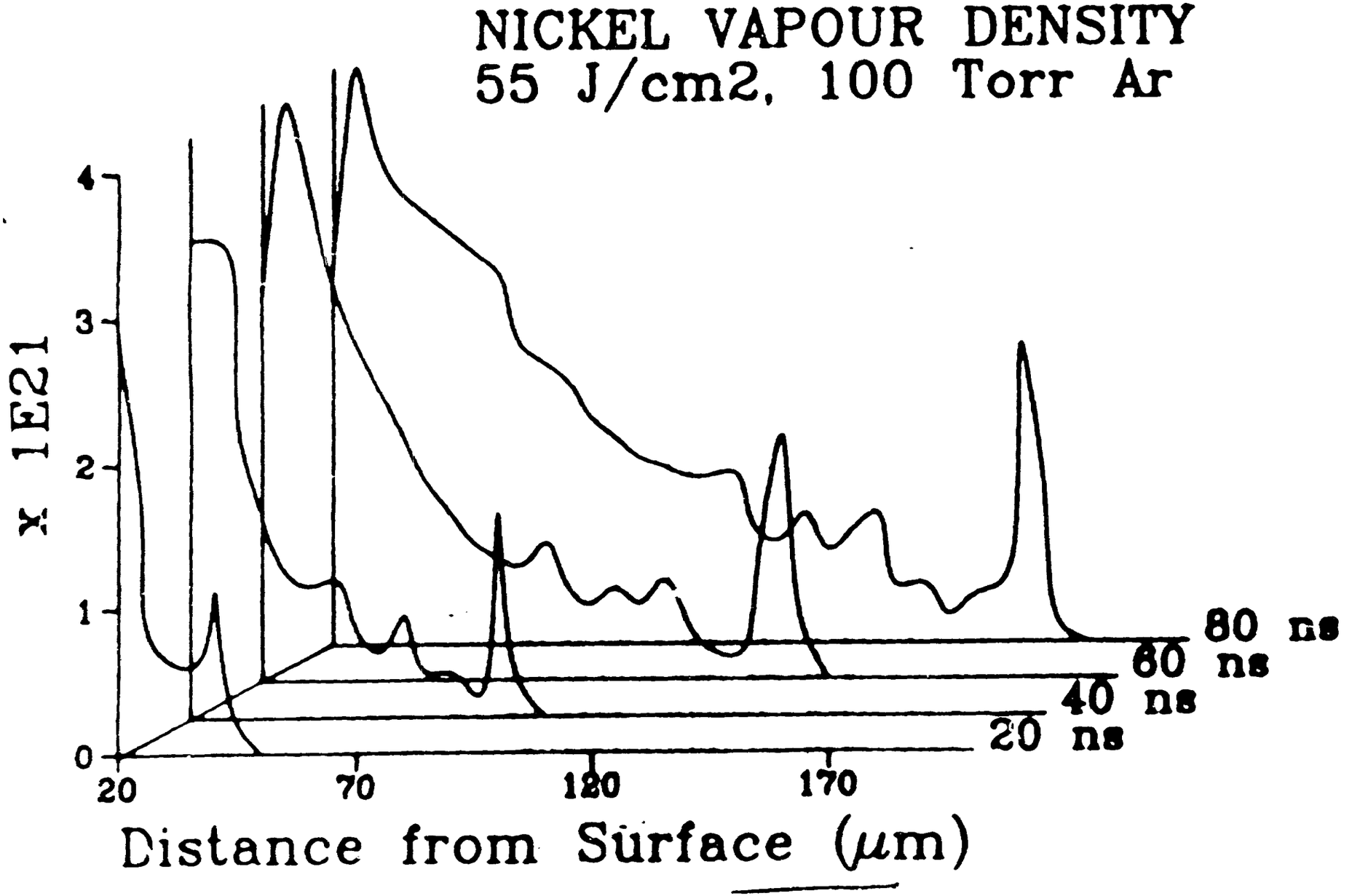
NICKEL VAPOUR DENSITY
55 J/cm2, 100 Torr Ar
X 1E21
0
1
2
3
4
20
70
120
170
Distance from Surface (μm)
80 ns
60 ns
40 ns
20 ns